STUDY ON THE ELECTROCHEMICAL PERFORMANCE OF FLOWER-LIKE ZNO NANOSTRUCTURE CRYSTALS FOR SUPERCAPACITOR APPLICATIONS

S. Nelson Amirtharaj[1,*] and M. Mariappan[2] and V. Beaula premavathi[3]

Abstract

A straightforward, low-cost process using cetyl trimethylammonium bromide (CTAB) as a templated sonochemical production method was used to create ZnO nanostructures with the appearance of flowers. Morphological characteristics of ZnO crystals have a greater impact on variables like the CTAB template and sonochemical reaction time. The synthetic strategy is easy to use and economical. The advantage of the flower-like ZnO crystals is the more active reaction centre, which improves redox processes and results in outstanding electrochemical attributes like high specific capacitance, good rate capability, and improved cyclic stability. The flower-like ZnO nanostructures (ZnO-2) deliver the specific capacitance of 425 Fg^{-1} at a scan rate of 5 mVs^{-1} from CV analysis whereas the charge/discharge study renders the specific capacitance of 426 Fg^{-1} at a current density of 1 Ag^{-1}. In long-term cyclic stability analysis, 89 % initial capacitance was retained after 3000 CV cycles at a scan rate of 100 mVs^{-1}. The distinctive flower-like ZnO nanostructures can be extended more for supercapacitor device applications.

Keywords: Sonochemical; CTAB; Flower -like ZnO; Supercapacitors; Energy storage

[1,*3] Department of Chemistry, T. B. M. L. College (Affiliated to Bharathidasan University,Thiruchirappali-24), Porayar, Tamilnadu 609307, India

[2]Department of Chemistry, Thiru. Vi. Ka. Govt. Arts College (Affiliated to Bharathidasan University, Thiruchirappali-24), Thiruvarur, Tamilnadu 610003, India

***Corresponding author:-** S. Nelson Amirtharaj

Department of Chemistry, T. B. M. L. College (Affiliated to Bharathidasan University, Thiruchirappali-24), Porayar, Tamilnadu 609307, India Email: *snelsamir@gmail.com*

DOI: 10.48047/ecb/2023.12.si10.00262

1introduction

Flower-like ZnO nanostructures were synthesized by a simple, inexpensive cetyl trimethylammonium bromide (CTAB) templated sonochemical preparation method. Till now, various transition metal oxides have been demonstrated as a pseudocapacitor electrode material. Because of its high specific capacitance, high conducting properties, and better environmental sustainability, ruthenium oxide (RuO_2) is commonly recognized as the primary active substance for pseudocapacitor electrode application[1,2]. Its low availability and poisonous nature have restricted its use in commercial applications, despite its high cost. As a result, lot of work has gone into developing different transition metal oxides such as MnO_2 [3], MoO_3 [4], SnO_2 [5], NiO[6], Co_3O_4 [7], ZnO[8] and V_2O_5 [9] materials. Recently, ZnO has drawn a lot of attention in the field of energy storage devices particularly in supercapacitors. Similarly, ZnO has excellent characteristics like wurtzite crystal structure, wide and direct bandgap, better binding energy (60 meV), optical, electrical, semiconductor and piezoelectric nature. ZnO has several benefits, including its availability, relatively inexpensive, low toxicity, and eco - friendliness[19,20]. These characteristics and benefits of ZnO make it a desirable substance for a variety of uses such as solar cells [10,11], light-emitting diodes [12,13], photovoltaic applications [14], solar water splitting [15] and photocatalysis [16]. As a result of its exceptional characteristics and electrical conductivity, ZnO is a substance of significant concern for supercapacitor applications. For instance, Lee et al [17] prepared various ZnO nanostructures through the chemical co-precipitation method and demonstrated their usage in electrochemical supercapacitor electrode application and exhibits the specific capacitance of 2.75 F g^{-1}. Huang et al [18] demonstrated the synthesis of ZnO microspheres from metal organic framework which exhibits the specific capacitance of 1017. 5 Fg^{-1} at a current density of 5 Ag^{-1}. Bishwakarma et al [19] prepared ZnO nanoparticles through hybrid machining process and examined its supercapacitor properties. It delivered 708. 75 Fg^{-1} at a current density of 1 Ag^{1} and it retained 90.42 % initial capacitance. Saranya et al established self-assembled flower-like mesoporous zinc oxide nanoflakes using hydrothermal method which deliver 322 Fg^{-1} at a scan rate of 5 mVs^{-1}.

In this endeavor, we demonstrate the simple and versatile synthetic approach to prepare ZnO flowers and it is utilized as a supercapacitor electrode material. The cetyl trimethyl mmonium bromide (CTAB) template was used to alter the morphology of the ZnO crystals. The XRD and FTIR techniques were used to analyze the crystalline structure and bonding properties of the ZnO materials. The supercapacitor features of freshly prepared ZnO flowers were analyzed through cyclic voltammetric, galvanostatic charge/discharge studies. The synthetic method is simple and cost-effective. These results indicated that the freshly prepared ZnO flowers are a significant candidate for supercapacitor application.

2 Experimental sections

2.1 Materials

All chemicals and reagents were used without purification and analytical grade. Zinc nitrate hexahydrate ($Zn(NO_3)_2{\cdot}6H_2O$), polyvinylidene difluoride (PVdF), carbon black and N-methyl-2-pyrrolidone were purchased from Sigma Aldrich, India. cetyl trimethyl ammonium bromide (CTAB) was procured from SRL (India). Potassium hydroxide, sodium hydroxide and stainless-steel foil were purchased from Alfa aeser.

2.2 Synthesis of ZnO crystals

The ZnO crystals were prepared by CTAB assisted sonochemical synthetic approach followed by the calcination process. In a distinctive preparation, the 100 ml water was taken in the separate beaker and 0.01 M of cetyltrimethylammonium bromide (CTAB) was dissolved in it. Then, the separate beaker containing 100 mL of DI water was taken and O.5 M of zinc nitrate hexahydrate was dissolved in it. After that, the zinc nitrate precursor solution was added to the CTAB solution and stirred for half an hour. In this precursor mixture, the precipitating agent such as 10 ml of 2 M NaOH was added and stirred for 20 min. to obtained the precipitation. After that, the precipitate was transferred to the ultrasonic bath and sonicate for 40 minutes. The resultant precipitates were collected by centrifugation process and washed completely with ethanol and deionized water respectively 80 °C for 10 h and it was annealed at 300 °C for 5h to attain the final samples. The sonication time was varied to 0, 20 and 40 minutes to attain ZnO-1, ZnO-2 and ZnO-3 samples.

2.3 preparation of electrodes for supercapacitor analysis

The electrochemical supercapacitive features were examined using cyclic voltammetric and galvanostatic charge/discharge analyses in a 1 M KOH electrolyte solution. The three-electrode

configuration was used to evaluate the electrochemical properties. The saturated calomel electrode, platinum foil, and ZnO coated steel foil current collector were utilized as reference counter and working electrodes respectively. The working electrode was prepared by the following procedure: At first, active material, carbon black and poly (vinylidene fluoride) (80:10:10) were taken in a mortar pestle and made a slurry with N-methyl-2-pyrrolidone (NMP) solvent. The slurry was coated on the stainless-steel foil and dried in a vacuum oven at 80 °C for 10 h. The resultant electrodes were used to analyze the supercapacitor studies. The weight of active material of the electrode materials is 4 mg.

3 Results and discussion

3.1 X-ray diffraction analysis

The material phase and crystalline nature of the freshly prepared ZnO crystals were evaluated utilizing XRD analysis and the corresponding results are displayed in figure 6.1. The sharp and high intensity peaks are perfectly visible in all XRD patterns, confirms that the high crystalline nature of the ZnO materials. The diffraction peaks shown at 31.8, 34.5, 36.3, 47.6, 56.7, 63, 66.5, 68.1, 69.2 72.7 and 77.1º are corresponds to (100), (002), (101), (102), (110), (103), (200), (112), (201), (004) and (202) planes respectively. The obtained planes are confirmed the formation of wurtzite hexagonal type ZnO structure with a space group of *P63mc* and it more consistent with the JCPDS card no.-01-075-0576. The wurtzite type of hexagonal structure is more stable when compared with zinc blende structure, which gives additional stability during the electrochemical cyclic stability analysis.

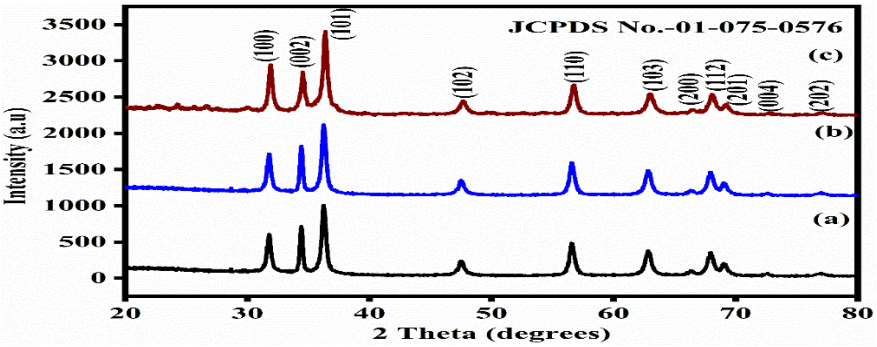

Figure 6.1: XRD analysis of (a) ZnO-1; (b) ZnO-2 and (c) ZnO-3 crystals

3.2 FTIR analysis

In particular, FTIR offers qualitative knowledge about the substance's functional groups and the vibrations of metal oxides. The FTIR analysis of the ZnO crystals prepared by the CTAB assisted sonochemical method is shown in figure6. 2. The peaks visible from 400 to 1000 cm^{-1} wavelengths are correspond to metal oxide peaks, which confirms the formation of ZnO materials[20,21]. The peaks at 428, 507 and 572 cm^{-1} are noticeable in the FTIR spectrum which is signature of the polar stretching vibrations and corresponds to *E1(TO)*, *A1(LO)* and *E1(LO)* modes respectively. The abovementioned three peaks are signifying the formation of ZnO crystals[22]. The peaks at 1023 and1325 cm^{-1} correspond to the presence of the CH_2 group and C-O-H bending mode respectively, which comes from the CTAB template. The peaks at 1621 and 3432 cm^{-1} are ascribed to stretching and bending vibrations of the O-H group respectively [23]. The FTIR and XRD pattern results signify the formation ZnO structure.

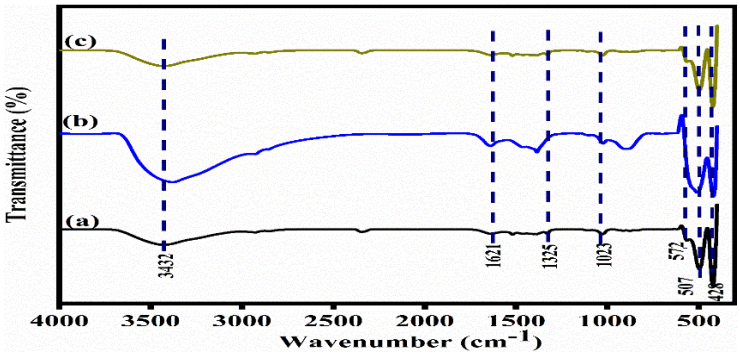

Figure 6.2: FTIR analysis of (a) ZnO-1; (b) ZnO-2 and (c) ZnO-3 crystals

3. 3 Morphological analysis

The surface textural properties of ZnO crystals were evaluated by HR-SEM analysis as shown in figure 6.3. Figure 6.3 a and b demonstrates the lower and higher magnification HR-SEM images of ZnO-1 material.

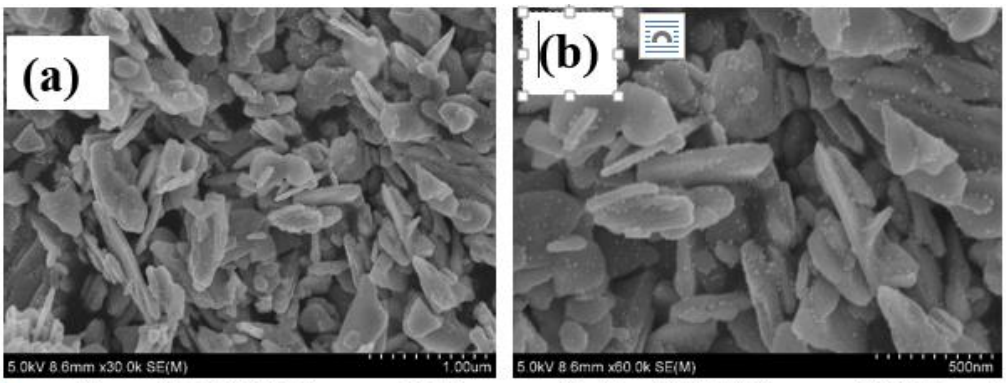

Figure 6.3 (a) & (b): Lower and higher magnification HR-SEM images of ZnO-1 crystal

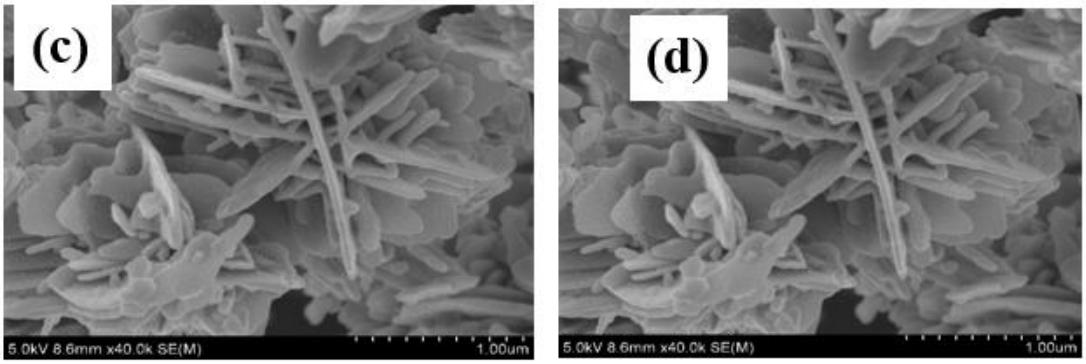

Figure 6.3 (c) & (d): Lower and higher magnification HR-SEM images of ZnO-2 crystal

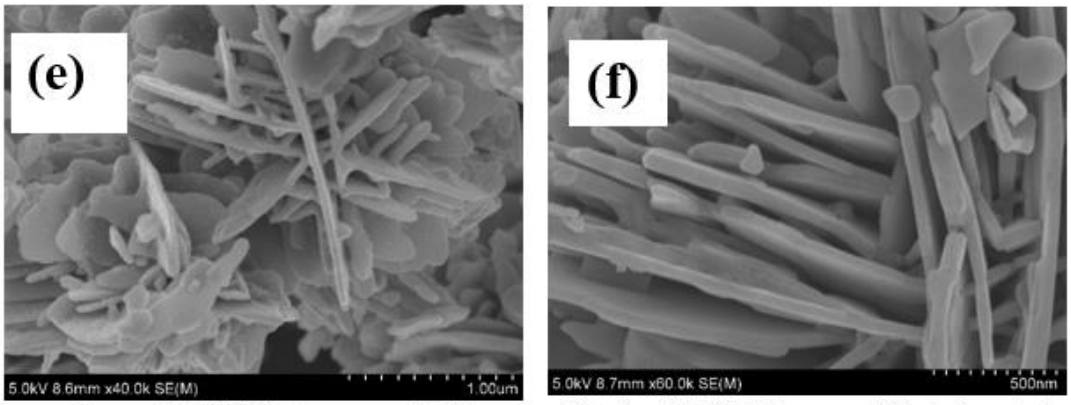

Figure 6.3 (e) & (f): Lower and higher magnification HR-SEM images of ZnO-3 crystal

The nanoplate structure is perfectly visible in both higher and lower magnification images. The breadth and size of the nanoplates are 350 ±10 nm and 60 ± 10 nm respectively. It is interesting to note that the small nanomaterials are uniformly formed on the surface of nanoplates. The ZnO flowers (ZnO-2) are formed when increasing ultrasound irradiation time to 20 minutes as shown in figure 6.3 c and d. The nanoplates are combined themselves and form flower-like structural morphologies. With the increase of irradiation time to 40 minutes (ZnO-3), the size of the ZnO flower is increased which is shown in Figures 6.3 e and f. More nanoplates are joined and show as the micro-sized flowers when increasing the ultrasound irradiation time from 20 to 40 minutes. The surface analysis signifies that the template and ultrasound irradiation time has influenced more during the material generation and provides ZnO flowers.

3.4 Electrochemical analysis

Various electrochemical tests, such as cyclic voltammetry (CV), cyclic stability, and

galvanostatic charge/discharge (CP) analysis, were executed on a three-electrode set-up, employing 1M KOH aqueous phase as the electrolyte to assess the performance of ZnO samples for supercapacitor electrode purposes. The CV analysis was recorded within a potential limit of 0-0.5 at various scan rates from 5 to 100 mVs^{-1} as shown in figure 6.4 a-c. These methods are commonly used to investigate the oxidation/reduction activity of processed electroactive material as well as their unique capacitive characteristics. Interestingly, during the cathodic and anodic sweeps of CV examination, a couple of very well redox peaks are generated, demonstrating the pseudocapacitive character of the prepared ZnO electroactive material. The generated pair of redox peaks are attributed to valence state changes related to the Zn (II)/Zn (III) transition arisen on the surface of ZnO electrodes[24]. It is worth noting that the redox peak potential of different prepared ZnO materials differed to some extent, which could be explained by the existence of varying surface morphological features[25].

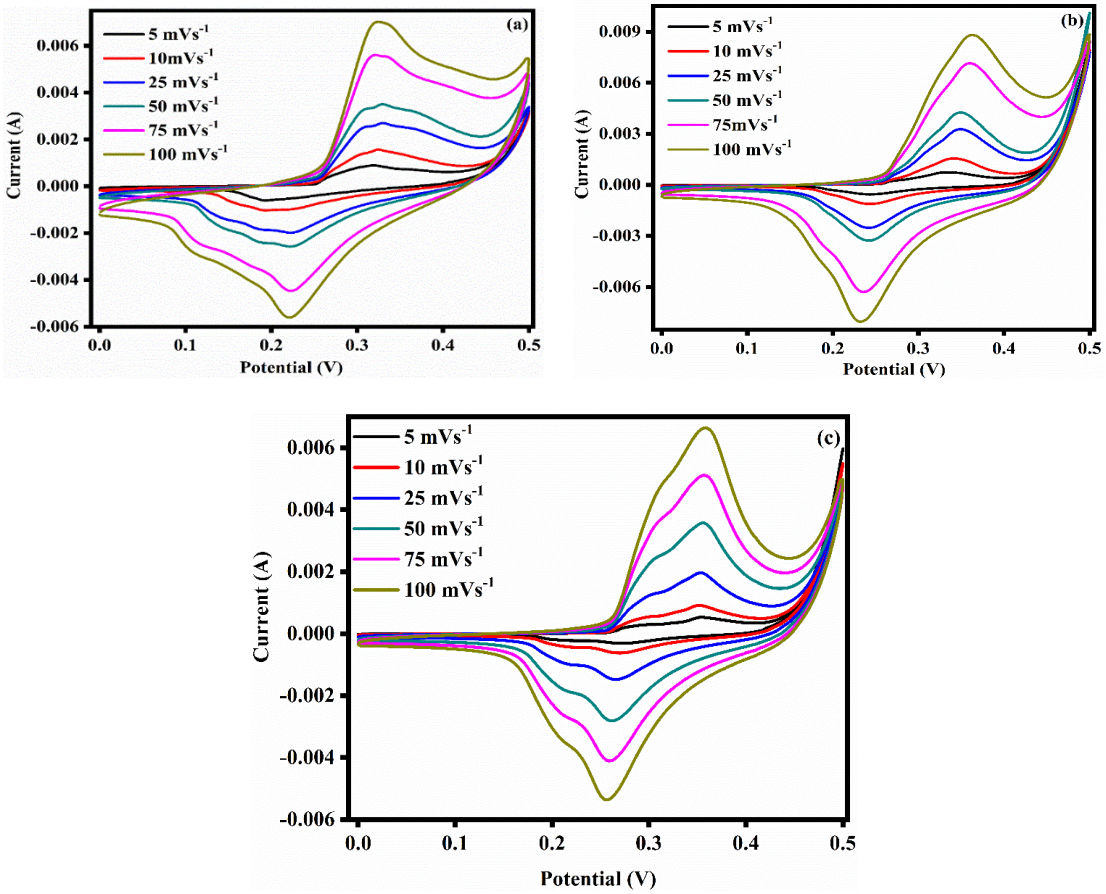

Figure 6. 4 : CV curve of (a) ZnO-1, (b) ZnO-2, (c) ZnO-3 electrode crystals

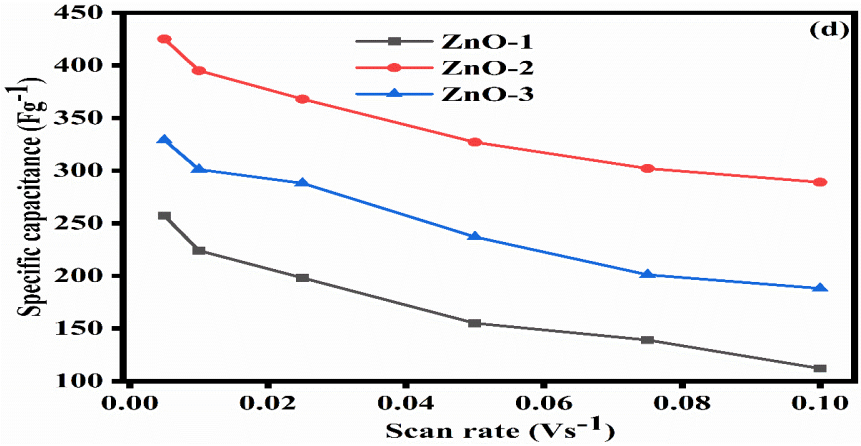

Figure 6. 4 (d): Specific capacitance vs scan rate graph of ZnO electrode crystals

The cathodic and anodic peak potentials and peak currents for all ZnO electrodes raised with increasing scan rate, signifying diffusion-controlled reaction kinetics and faster electronic and ionic transport at the interface of electrolyte and electrode materials [26]. The rate capability of the ZnO electrode was also tested with scan rates ranging from 5 to 100 mVs^{-1}. The observation that well-defined redox peaks can be observed even at faster scan rates indicates that prepared ZnO specimens are resistant to fast redox reactions[38]. The unique capacitance character is directly proportional to the area under the CV curve of active materials. Interestingly, ZnO-2 electrode has a large area under the CV curve when compared to ZnO-1 and ZnO -3 electrodes, demonstrating that the ZnO-3 electrodes have a superior basic capacitive feature. Equation 1 is used to calculate the specific capacitance of CV curves.

$$Cs = \frac{\int idv}{2*S*M*V} \quad (1)$$

Where *Cs* is the specific capacitance (Fg^{-1}), $\int idV$ is the integrated area of CV curves, S the scan rate ($mV\ s^{-1}$), M is the active mass (g), and V is the potential window (V). ZnO-1 and ZnO -2 and ZnO-3 electrodes deliver the specific capacitance of 257, 425 and 329 Fg^{-1} respectively. Among all the ZnO materials, ZnO-2 provides superior capacitance than ZnO-1 and ZnO -3 materials. Figure 6.4 d shows the scan rate vs specific capacitance graph. It is apparent that the specific capacitance increases with the rising of scan rate from 5 to 100 mVs^{-1}. The observation that real capacitance lowers with rising current density may be attributed to low electrolyte ion diffusion on electrode surfaces. At high scan rates, only the external surface region of the electrode materials is included in the electrochemical phase, limiting the electroactive substance usage, while at lower current densities, there might be enough time for a redox reaction to proceed both in the inner and outer surface regions of the electrode substance, allowing for greater electroactive substance utilization[27].The galvanostatic charge/discharge analysis was recorded for ZnO materials within a voltage limits from 0 to 0.45 V at different current densities such as 1, 2, 3, 10 and 30 Ag^{-1} as shown in figure 6.5 a-c. All the charge-discharge curves deviate significantly from a rectangular behavior and show the non-linear profile, demonstrating that capacitive activity is caused by a faradic redox reaction[28]. The fact that all of the charge/ discharge curves have small iR lass means that ZnO materials have good capacitive features. The charge/discharge curve of the ZnO- 2 electrode has a longer duration than the other electrode manO-1 and ZnO-3. This trend supports the ZnO- 2 electrode's high specific capacitance behavior. Equation 2 is utilized to calculate the specific capacitance from charge/discharge curves.

$$Cs = \frac{I\Delta t}{m\Delta V} \quad (2)$$

Where I, Δt, m and ΔV is representing the current density (Ag^{-1}), discharge time (s), the mass of the active materials and the potential window. The calculated specific capacitance values are 255, 426 and 307 Fg^{-1} for ZnO-1, ZnO-2 and ZnO-3 electrodes respectively at a current density of 1 Ag^{-1}. The higher specific capacitance values are due to the flower-like nanostructure of the current ZnO-2 electrode material, which contributes to good electrolyte penetration, resulting in shorter OH^- ion diffusion time and more usable spaces for redox reactions. Further more, The ZnO flowers, which are made up of centrifugally self-assembled nanoplates, can significantly improve the electrode/electrolyte contact area and speed up electron and ion movement. Since every plate is in interaction with the electrolyte, the open space between the neighboring plates allows for quick diffusion of the electrolyte, ensuring that each sheet can contribute to the electrochemical process. The ZnO-3 materials deliver lower capacitance when compared with ZnO-2 materials, which due to the larger size ZnO flower structure and the small gap between neighborhood plates restricts the ion transport and it reduced the specific capacitance.

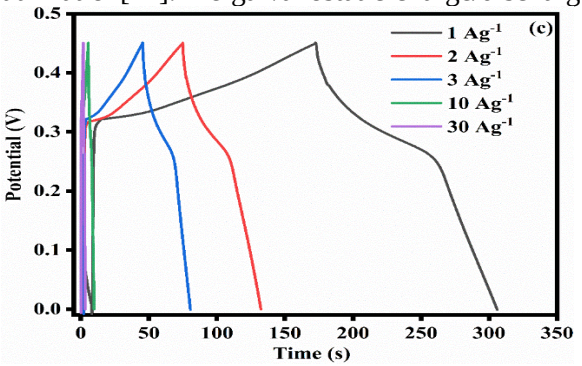

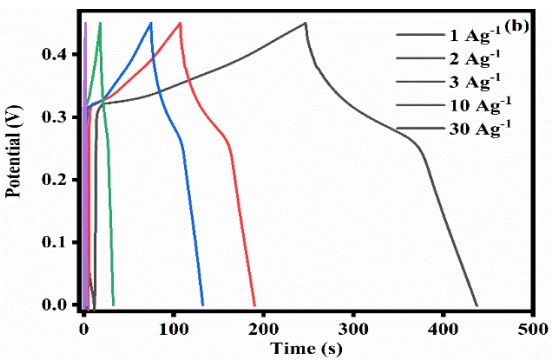

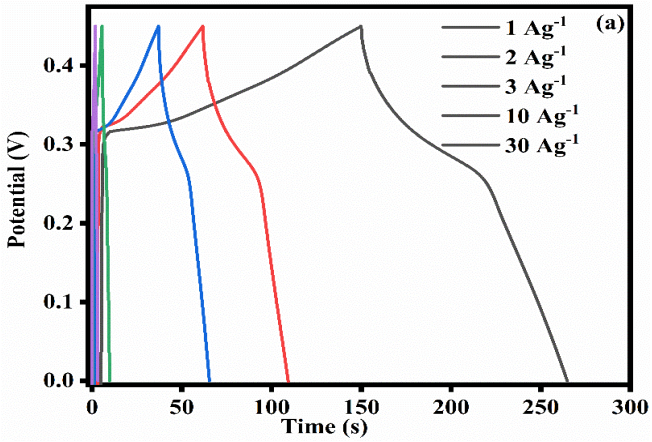

Figure 6. 5 : GCD curves of (a) ZnO-1, (b) ZnO-2, (c) ZnO-3 electrode crystals

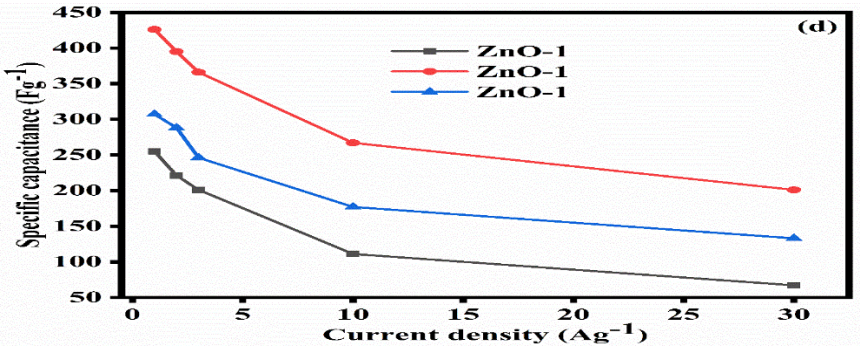

Figure 6. 5 (d): Specific capacitance vs current density graphs of ZnO electrode crystals

The current density vs specific capacitance graph is shown in fig.6.5 (d). When the current density is low, the capacitance is large, but as the current density rises, the capacitance reduces. The drop in capacitance is primarily due to a decrease in voltage drop in discharge curves as current density increases, as well as slow reaction kinetics at the interface of electrolyte/electrode materials. The energy and power density parameters of supercapacitors are quite important for device fabrication. Charge/discharge profiles can be used to measure energy and power densities, which are measured using the equations (3) and (4) respectively.

$$E = \frac{1}{2}\frac{C \times V^2}{3.6} \qquad (3)$$

$$P = \frac{E \times 3600}{t} \qquad (4)$$

Where *E*, *C*, *V*, *P* and *t* represent energy density (Wh Kg^{-1}), specific capacitance (F g^{-1}), Potential window (V), power density (W Kg^{-1}), and discharge time respectively. The energy density vs power density graph is shown in figure 6. 6. The energy density values of 7, 12 and 8.6 Wh Kg^{-1} were offered by the ZnO-1, ZnO-2 and ZnO-3 materials respectively. Furthermore, the power density values such as 3600, 6720, 6660 W Kg^{-1} were obtained from ZnO-1, ZnO-2 and ZnO-3 electrodes respectively. The flower structure of ZnO-2 electrodes delivers higher energy and power densities than ZnO-1 and ZnO-2 materials due to its unique morphological properties. Cycling stability is a major necessity for supercapacitors and it explores by 3000 continuous CV cycles at a scan rate of 100 mVs^{-1}. The cyclic stability studies of ZnO-1, ZnO-2 and ZnO-3 electrodes are shown in figure 6.7 a. The figures 6.7 (b, c and d) are corresponds to 1st and 3000th cycles of cyclic stability studies for ZnO-1, ZnO-2 and ZnO-3 respectively. It can be shown that the preliminary specific capacitance increases steadily over 800 cycles, which can be due to the complete activation process of the current ZnO electrodes [29]. After that, the specific apacitances are gradually decreased and withstand 80 (ZnO-1), 89 (ZnO-2) and 84 % (ZnO-3) of initial capacitance after 3000 consecutive cycles. The ZnO-2 electrode delivers superior cyclic stability than ZnO-1 and ZnO-3 electrodes implies that the ZnO-2 flowers be more advantageous than other morphologies for improving electrochemical efficiency.

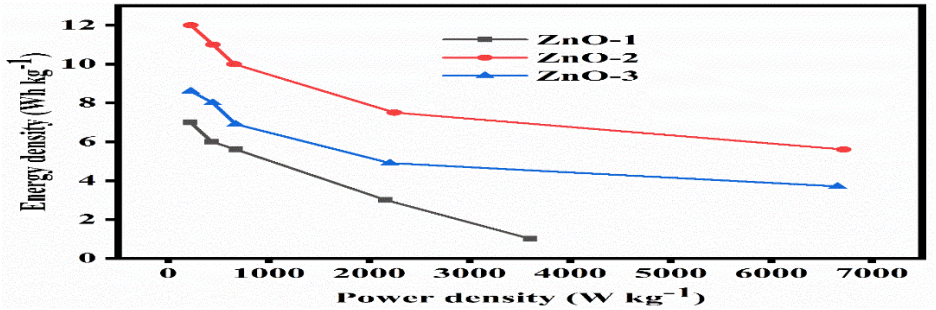

Figure 6. 6: Energy density vs power density of ZnO-1; ZnO-2 and ZnO-3 materials

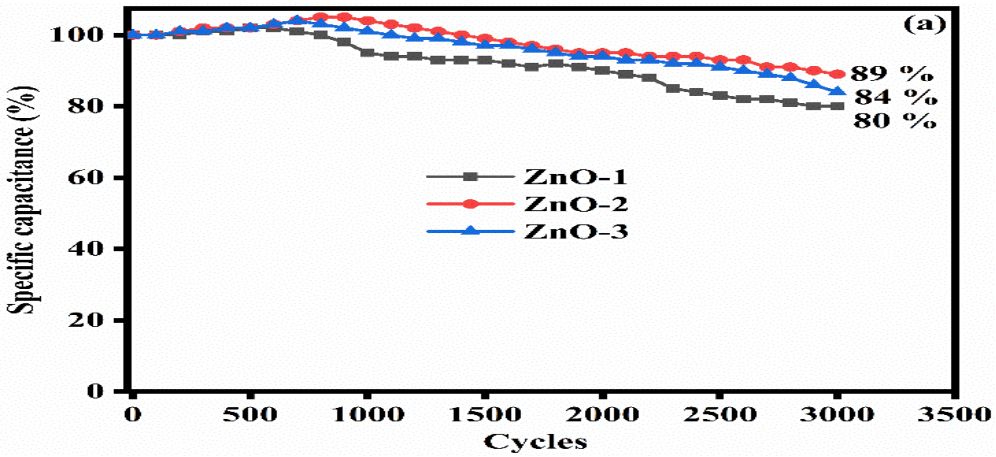

Figure 6. 7 (a): Cyclic stability studies of (a) ZnO-1, ZnO-2 and ZnO-3 materials

.

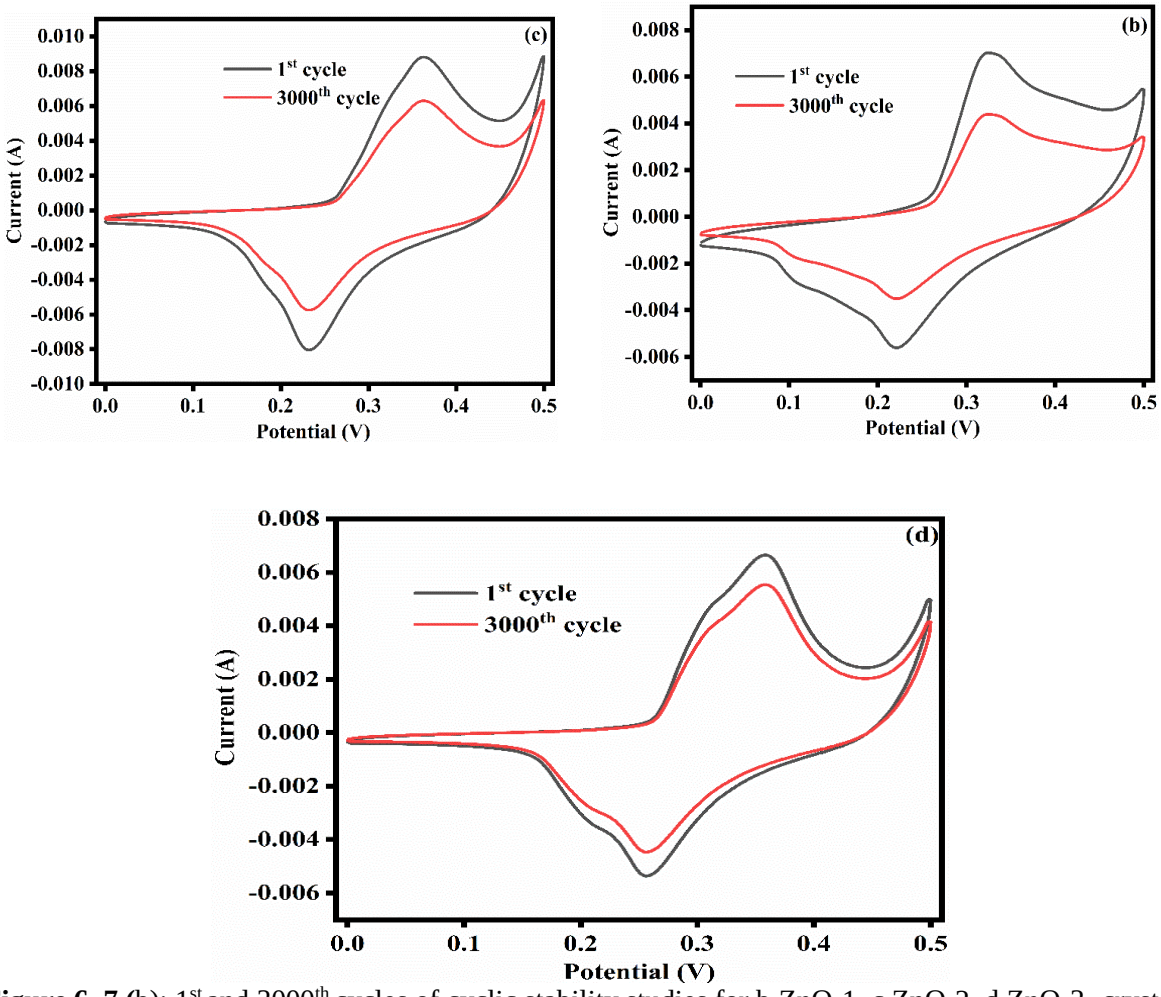

Figure 6. 7 (b): 1st and 3000th cycles of cyclic stability studies for b ZnO-1, c ZnO-2, d ZnO-3- crystal

4 Conclusion

A facile, CTAB assisted sonochemical approach was followed to generate flower-like ZnO nanostructures. The factors such as the CTAB template and sonochemical reaction time are more influenced by the morphological properties of ZnO crystals. The synthetic approach is simple and cost-effective. The more active reaction center is the beneficial feature of flower-like ZnO materials which provide better redox reactions leading to excellent electrochemical properties such as high specific capacitance, good rate capability, and enhanced cyclic stability. The flower-like ZnO nanostructures (ZnO-2) deliver the specific capacitance of 425 Fg^{-1} at a scan rate of 5 mVs^{-1} from CV analysis whereas the charge/discharge study renders the specific capacitance of 426 Fg^{-1} at a current density of 1 Ag^{-1}. In long-term cyclic stability analysis, 89 % initial capacitance was retained after 3000 CV cycles at a scan rate of 100 mVs^{-1}. The distinctive flower-like ZnO nanostructures can be extended more for supercapacitor device applications.

References

1. C.C. Hu, K.H. Chang, M.C. Lin, Y.T. Wu, Design and tailoring of the nanotubular arrayed architecture of hydrous RuO_2 for next generation supercapacitors, Nano Lett. 6 (2006) 2690–2695. https://doi.org/10.1021/nl061576a.
2. V. Subramanian, S.C. Hall, P.H. Smith, B. Rambabu, Mesoporous anhydrous RuO_2 as a supercapacitor electrode material, Solid State Ionics. 175 (2004) 511–515. https://doi.org/ 10.1016/j.ssi.2004.01.070.
3. S. Zhao, T. Liu, D. Hou, W. Zeng, B. Miao, S. Hussain, X. Peng, M.S. Javed, Controlled synthesis of hierarchical birnessite-type MnO_2 nanoflowers for supercapacitor applications, Appl. Surf. Sci. 356 (2015) 259–265. https:// doi.org/10.1016/j.apsusc.2015.08.037.
4. J.C. Icaza, R.K. Guduru, Characterization of α-MoO_3 anode with aqueous beryllium sulfate for supercapacitors, J. Alloys Compd. 726 (2017) 453–459. https://doi.org/ 10.1016/ j.jallcom.2017.08.031.
5. V. Bonu, B. Gupta, S. Chandra, A. Das, S. Dhara, A.K. Tyagi, Electrochemical supercapacitor performance of SnO_2 quantum dots, Electrochim. Acta. 203 (2016) 230–237. https://doi.org/10.1016/j.electacta.2016.03.153 .
6. G. Anandha Babu, G. Ravi, T. Mahalingam, M. Kumaresavanji, Y. Hayakawa, s of microwave power on the preparation of NiO nanoflakes for enhanced magnetic and supercapacitor applications, Dalt. Trans. 44 (2015) 4485–4497. https://doi.org/ 10.1039/.
7. R. Poongodi S. Sengutuvan and R. Sagayaraj Role of annealing temperature in tuning magnetic properties of Fe-Co-Al_2O_4 spinel aluminates, Asian Journal of chemistry. Vol. 35,No.6(2023), 1525-153. https://doi.org/10.14233/ajchem.2023.27625.
8. G. Theophil Anand, D. Renuka, R. Ramesh, L. Anandaraj, S. John Sundaram, G. Ramalingam, C.M. Magdalane, A.K.H. Bashir, M. Maaza, K. Kaviyarasu, Green synthesis of ZnO nanoparticle using Prunus dulcis (Almond Gum) for antimicrobial and supercapacitor applications, Surfaces and Interfaces. 17 (2019) 100376. https://doi.org/10.1016/ j.surfin.2019. 100376.
9. J. Yang, T. Lan, J. Liu, Y. Song, M. Wei, Supercapacitor electrode of hollow spherical V_2O_5 with a high pseudocapacitance in aqueous solution, Electrochim. Acta. 105 (2013) 489–495. https://doi.org/10.1016/j. electacta. 2013. 05. 023.
10. M. Selvakumar, D. Krishna Bhat, A. Manish Aggarwal, S. Prahladh Iyer, G. Sravani, Nano ZnO-activated carbon composite electrodes for supercapacitors, Phys. B Condens. Matter. 405 (2010) 2286–2289. https://doi.org/10.1016/j.physb.2010.02.028.
11. X. Li, Z. Wang, Y. Qiu, Q. Pan, P. Hu, 3D graphene/ZnO nanorods composite networks as supercapacitor electrodes, J. Alloys Compd. 620 (2015) 31–37. https://doi.org/ 10.1016/ j.jallcom.2014.09.105.
12. K. Keis, C. Bauer, G. Boschloo, A. Hagfeldt, K. Westermark, H. Rensmo, H. Siegbahn, Nanostructured ZnO electrodes for dye-sensitized solar cell applications, J. Photochem. Photobiol. A Chem. 148 (2002) 57–64. https:// doi.org/10.1016/S1010-6030(02)00039-4.
13. K. Matsubara, P. Fons, K. Iwata, A. Yamada, K. Sakurai, H. Tampo, S. Niki, ZnO transparent conducting films deposited by pulsed laser deposition for solar cell applications, Thin Solid Films. 431–432 (2003) 369–372. https://doi.org/10.1016/S0040-6090 (03)00243-8.
14. D.K. Hwang, M.S. Oh, J.H. Lim, S.J. Park, ZnO thin films and light-emitting diodes, J. Phys. D. Appl. Phys. 40 (2007). https://doi.org/ 10. 1088/0022-3727/40/22/R01.
15. S.J. Pearton, F. Ren, Advances in ZnO-based materials for light emitting diodes, Curr. Opin. Chem. Eng. 3 (2014) 51–55. https:// doi. org/10.1016/j.coche.2013.11.002.

16. K. Keis, L. Vayssieres, S.E. Lindquist, A. Hagfeldt, Nanostructured ZnO electrodes for photovoltaic applications, Nanostructured Mater. 12 (1999) 487–490. https://doi.org/ 10.1016/S0965-9773(99)00165-8.
17. P.R. Deshmukh, Y. Sohn, W.G. Shin, Chemical synthesis of ZnO nanorods: Investigations of electrochemical performance and photo-electrochemical water splitting applications, J. Alloys Compd. 711 (2017) 573–580. https://doi.org/10.1016/j.jallcom.2017.04.030.
18. V. Oskoei, M.H. Dehghani, S. Nazmara, B. Heibati, M. Asif, I. Tyagi, S. Agarwal, V.K. Gupta, Removal of humic acid from aqueous solution using UV/ZnO nano-photocatalysis and adsorption, J. Mol. Liq. 213 (2016) 374–380. https://doi.org/10.1016/ j.molliq.2015.07.052.
19. K.S. Lee, C.W. Park, J.D. Kim, Electrochemical properties and characterization of various ZnO structures using a precipitation method, Colloids Surfaces A Physicochem. Eng. Asp. 512 (2017) 87–92. https://doi.org/10. 1016/j.colsurfa.2016.10.022.
20. G. Huang, W. Zhang, S. Xu, Y. Li, Y. Yang, Microspherical ZnO synthesized from a metal-organic precursor for supercapacitors, Ionics (Kiel). 22 (2016) 2169–2174. https://doi. org/10.1007/s11581-016-1745-7.
21. H. Bishwakarma, A.K. Das, Synthesis of Zinc Oxide Nanoparticles Through Hybrid Machining Process and Their Application in Supercapacitors, J. Electron. Mater. 49 (2020) 1541–1549. https://doi.org/ 10.1007/s 11664-019-07835-x.
22. M. Faisal, S.B. Khan, M.M. Rahman, A. Jamal, A.M. Asiri, M.M. Abdullah, Synthesis, characterizations, photocatalytic and sensing studies of ZnO nanocapsules, Appl. Surf. Sci. 258 (2011) 672–677. https://doi.org/10.1016/ j.apsusc.2011.07.067.
23. Q. Yuan, S. Hein, R.D.K. Misra, New generation of chitosan-encapsulated ZnO quantum dots loaded with drug: Synthesis, characterization and in vitro drug delivery response, Acta Biomater. 6 (2010) 2732–2739. https://doi.org/10.1016/ j.actbio.2010. 01.025.
24. A. Sahai, N. Goswami, Structural and vibrational properties of ZnO nanoparticles synthesized by the chemical precipitation method, Phys. E Low-Dimensional Syst. Nanostructures. 58 (2014) 130–137. https://doi. org/10.1016/j.physe.2013.12.009.
25. A.S. Lanje, S.J. Sharma, R.S. Ningthoujam, J.S. Ahn, R.B. Pode, Low temperature dielectric studies of zinc oxide (ZnO) nanoparticles prepared by precipitation method, Adv. Powder Technol. 24 (2013) 331–335. https://doi.org/10.1016/j.apt.2012.08.005.
26. P.E. Saranya, S. Selladurai, Facile Synthesis of Self-Assembled Flower-Like Mesoporous Zinc Oxide Nanoflakes for Energy Applications, Int. J. Nanosci. 17 (2018) 1–13. https://doi.org/10.1142/S0219581X1760002X.
27. X. Wang, M. Li, Z. Chang, Y. Wang, B. Chen, L. Zhang, Y. Wu, Orientated Co_3O_4 Nanocrystals on MWCNTs as Superior Battery-Type Positive Electrode Material for a Hybrid Capacitor, J. Electrochem. Soc. 162 (2015) A1966–A1971. https://doi.org/10.1149/ 2.0041511jes.
28. J. Zhang, H. Feng, Q. Qin, G. Zhang, Y. Cui, Z. Chai, W. Zheng, Interior design of three-dimensional CuO ordered architectures with enhanced performance for supercapacitors, J. Mater. Chem. A. 4 (2016) 6357–6367. https://doi.org/10.1039/C6TA00397D.
29. A.A. Kashale, M.M. Vadiyar, S.S. Kolekar, B.R. Sathe, J.Y. Chang, H.N. Dhakal, A. V. Ghule, Binder free 2D aligned efficient MnO_2 micro flowers as stable electrodes for symmetric supercapacitor applications, RSC Adv. 7 (2017) 36886–36894. https://doi.org/ 10.1039/c7ra05655a.